atmosphere

MDPI

Article

Estimating Terrestrial Radiation for Human Thermal Comfort in Outdoor Urban Space

Kanghyun Lee [1,*] and Robert D. Brown [2]

[1] Division of Landscape Architecture, College of Architecture, University of Oklahoma, Norman, OK 73019, USA
[2] Department of Landscape Architecture and Urban Planning, College of Architecture, Texas A&M University, College Station, TX 77843, USA; robert.brown@tamu.edu
* Correspondence: kanghyun.lee@ou.edu

Abstract: Cities inadvertently create warmer and drier urban climate conditions than their surrounding areas through urbanization that replaces natural surfaces with impervious materials. These changes cause heat-related health problems and many studies suggest microclimatic urban design (MUD) as an approach to address these problems. In MUD-related research, although terrestrial radiation plays an important role in human thermal comfort and previous studies use thermal comfort models to identify human heat stress, few studies have addressed the effect of terrestrial radiation. This study develops the ground ratio factor (GRF) model to estimate the different terrestrial radiation according to different ground conditions. Three types of ground materials (asphalt, concrete, and grass) were considered in the model, and field studies were conducted in humid subtropical climate (Cfa) zone during the hot season (13 July to 19 September 2020). The model was validated by comparing the predicated terrestrial radiation (PTR) from the model with the actual terrestrial radiation (ATR). The results showed that there is a statistically significant strong correlation between PTR and ATR. The model can contribute to MUD strategies by updating existing human energy budget models, which can lead to the measurement of more accurate human thermal comfort for mitigating thermal environments.

Keywords: microclimatic urban design; terrestrial radiation; human thermal comfort; ground ratio factor

Citation: Lee, K.; Brown, R.D. Estimating Terrestrial Radiation for Human Thermal Comfort in Outdoor Urban Space. *Atmosphere* **2021**, *12*, 1701. https://doi.org/10.3390/atmos12121701

Academic Editors: Dragan Milosevic, Britta Jänicke, Yuliya Dzyuban and Michael Allen

Received: 18 November 2021
Accepted: 7 December 2021
Published: 19 December 2021

1. Introduction

There is no doubt that global climate change is causing serious urban warming (Limaye et al. 2018) and due to the rapid urbanization, cities often inadvertently create warmer and drier urban climate conditions than their surrounding areas, which is known as the urban heat island (UHI) phenomenon. These thermal environments cause heat-related health problems [1,2]. Meanwhile, heat stress, which can be assessed by human energy budget models, plays an important role in causing heat-related health. According to Epstein and Moran [3], various age groups, including infants, children, and adults over 65, are most vulnerable to heat-related death since they are more sensitive to excessive heat stress. Heat stress can also reduce workers' productivity and cause more serious heat-health problems, especially in vulnerable groups [4].

While individuals have little control over the impact of global issues on heat-related health, there is evidence that urban design ameliorates health problems by increasing human thermal comfort and contributing to reduced heat stress at the urban level [5,6]. In this regard, researchers suggest microclimatic urban design (MUD), which is the process of determining the physical organization of buildings and open spaces in urban areas to mitigate thermal environments [7]. Many studies are underway on MUD and they have found that MUD has positive impacts on urban microclimate and heat-related health [8].

Their strategies focus on green areas [9,10], surface of building and pavement [5,11], water bodies [12–14], and structure of streets and buildings [15,16] at the micro- and mesoscale.

According to the MUD-related research, terrestrial radiation plays an important role in outdoor human thermal comfort. Brown and Gillespie [17] demonstrated the effect of terrestrial radiation on human thermal comfort through the COMFA model. They found that terrestrial radiation absorbed by a person has negative effects on human thermal comfort during the hot summer weather. All of the materials on Earth emit invisible terrestrial radiation as a function of their surface temperature [18], and the warmer the object is, the more terrestrial radiation it emits. This invisible energy has a significant effect on outdoor human thermal comfort. Moreover, Shahidan et al. [18] demonstrated that the solar radiation filtering capacity of trees reduces the terrestrial radiation by cooling the ground, and it is related to improve outdoor thermal comfort in tropical open spaces.

Among the MUD elements, including green, surface, water body, and urban structure, terrestrial radiation is related to the surface. However, surface-related studies have mostly focused on the energy that varies with the albedo of different ground materials, and has rarely considered the amount of terrestrial radiation emitted. Moreover, previous studies have used thermal comfort models to calculate energy budgets that can identify the thermal stress level [19], and there have been 165 thermal indices developed for estimating indoor and outdoor thermal comfort levels [20]. However, the impact of terrestrial radiation is not considered in most of the existing models. The existing models typically use air temperature, solar radiation, relative humidity, and wind speed as the main microclimate parameters. For example, Coccolo et al. [21] conducted a comprehensive review of models and standards of outdoor thermal comfort and stress. A total of 21 thermal comfort models were analyzed in their study. Among them, 11 models consider solar radiation, 21 models consider air temperature, 19 models consider relative humidity, and 15 models consider wind speed. Only one model, the COMFA, considers the terrestrial radiation absorbed by a person, but it does not take into account the surrounding ground conditions at the point where the subject is standing. It only considers the terrestrial radiation of the point where the subject is standing.

By developing a model which can consider the various ground conditions, the ground ratio (GR) of each material, and their terrestrial radiation, this study can contribute to creating MUD strategies by updating existing energy budget models, which can lead to the measurement of more accurate human thermal comfort. Therefore, the goals of the study are to (1) present the need to consider terrestrial radiation for human energy budgets, (2) develop a ground ratio factor (GRF) model that can estimate the difference in terrestrial radiation according to different ground conditions, (3) validate the GRF model through field testing, and (4) propose how the model can be used in microclimatic urban design to ameliorate urban heat islands.

2. Methods

2.1. Ground Ratio Factor (GRF) Model

2.1.1. GRF

Terrestrial radiation will be emitted differently depending on ground conditions. For example, a person standing on a place with 95% concrete and 5% grass will absorb more terrestrial radiation from the ground than a person standing on a place with 100% grass. This is due to the fact that concrete emits more energy in hot weather since it has a higher temperature than grass (Figure 1). Therefore, GRF represents the ratio of different ground materials to the location where a person is standing. In this study, the spatial range of GRF was a radius of 3 m from where a person is standing. The CNR4 instrument used to measure terrestrial radiation has a lower detector with a view of 150 degrees. Theoretically, a detector with a view of 150 degrees installed at a height of 1.5 m has a measurable range of a radius of 5.6 m. However, the actual measurements showed that the measurable range was a radius of 3 m. The range has been established for the analysis of this study. The application of additional space is possible depending on the results of the study.

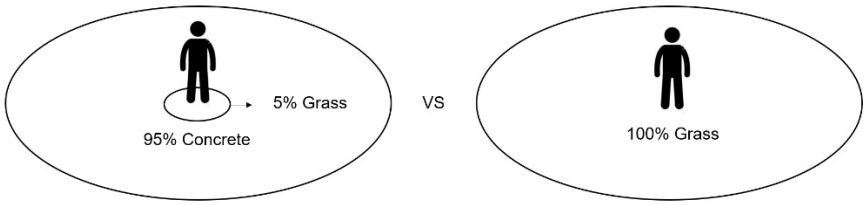

Figure 1. Concept of GRF.

2.1.2. GRF Model

To develop better thermal comfort models, this study attempted to develop the GRF model that can calculate the different terrestrial radiation depending on the ground cover ratio of various materials (Figure 2). Austrian physicists Stefan-Boltzmann, who made a significant contribution to radiation and gases theory in the late 19th century, suggested that energy-temperature relations should follow the law when the temperature is in Celsius degrees (Equation (1)). According to the law, terrestrial radiation can be calculated by the surface (ground) temperature.

$$Energy = \sigma\ (\mathrm{T} + 273)^4 \tag{1}$$

where σ (Greek letter sigma) represents the constant of proportionality, called the Stefan-Boltzmann constant. This constant has a value of 5.67×10^{-8} watt per meter squared per kelvin to the fourth ($\mathrm{W/m^2\ K^4}$). T is the ground temperature in Celsius degrees.

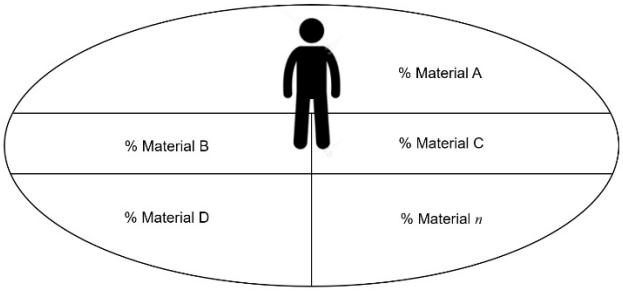

Figure 2. Concept of the GRF model with various ground materials.

1. Ground temperature-based GRF (GRF-G) model

The Stefan-Boltzmann law was used to develop the model. The amount of different terrestrial radiation depending on the ground cover ratio of various materials can be calculated by the GRF-G model (Equation (2)). The ground temperature of various materials can be used in the model. To calculate the ground ratio (GR), a radius of 3 m from where a person stands is considered. GR values are from 0 to 100%. Then, the amount of terrestrial radiation emitted by each different ground material was multiplied by the GR of the corresponding material.

$$\begin{aligned} R_T = {} & \text{ Material A's GR } \times \sigma\ (T_{AG} + 273)^4 + \text{ Material B's GR } \times \sigma\ (T_{BG} + 273)^4 \\ & + \text{ Material C's GR } \times \sigma\ (T_{CG} + 273)^4 + \text{ Material D's GR } \times \sigma\ (T_{DG} + 273)^4 + \\ & \ldots + \text{ Material n's GR } \times \sigma\ (T_{nG} + 273)^4 \end{aligned} \tag{2}$$

where R_T is the predicted terrestrial radiation ($\mathrm{W/m^2}$), σ is the constant of proportionality with a value 5.67×10^{-8} $\mathrm{W/m^2\ K^4}$, GR is the ground ratio, and T_{AG} is the ground temperature of material A, T_{BG} is the ground temperature of material B, T_{CG} is the ground temperature of material C, T_{DG} is the ground temperature of material D, and T_{nG} is the ground temperature of material n in Celsius degrees.

2. Air Temperature-based GRF (GRF-A) Model

Air temperature data can be easily obtained through local weather stations, but ground temperature data are generally not available [22]. Since only ground temperature can be used in the model, an air temperature-based model was developed by converting air temperature to ground temperature. To estimate the ground temperature, regression analysis was used for each of the three ground materials (Equation (3)). Shamsipour et al. [23] and Ariawan et al. [24] proposed the regression analysis to estimate ground temperature using air temperature. The ground temperature was used as a dependent variable and the air temperature as an independent variable. The results of the regression analysis for asphalt, concrete, and grass were applied to the GRF-G model (Equation (4)).

$$Y_i = \beta_0 + \beta_1 X_i + \varepsilon_i \tag{3}$$

where Y_i is the dependent variable (ground temperature), β_0 is the population Y intercept, β_1 is the population slope coefficient, X_i is the independent variable (air temperature), and ε_i is the random error term.

$$\begin{gathered} R_T = Material\ A's\ GR \times \sigma\ (Y_A + 273)^4 + Material\ B's\ GR \times \sigma\ (Y_B + 273)^4 \\ + Material\ C's\ GR \times \sigma\ (Y_C + 273)^4 + Material\ D's\ GR \times \sigma\ (Y_D + 273)^4 + \ldots \\ + Material\ n's\ GR \times \sigma\ (Y_n + 273)^4 \end{gathered} \tag{4}$$

where R_T is the predicted terrestrial radiation (W/m^2), σ is the constant of proportionality with a value of 5.67×10^{-8} W/m^2 K^4, GR is the ground ratio, and Y_A is the ground temperature of material A obtained from the regression analysis, Y_B is the ground temperature of material B obtained from the regression analysis, Y_C is the ground temperature of material C obtained from the regression analysis, Y_D is the ground temperature of material D obtained from the regression analysis, and Y_n is the ground temperature of material n obtained from the regression analysis in Celsius degrees.

2.2. Field Study

Microclimate data may vary depending on the climate zone, time, and season [25]. Therefore, the scope of the study was narrowed to the Cfa climate zone (humid subtropical climate) from the Köppen climate classification. The City of College Station, Texas, which is located in the Cfa climate zone, was selected for the study. College Station has an hot and humid weather in the summer and a cold and mild weather in the winter.

To develop the model, three types of ground materials were selected: Asphalt, concrete, and grass. They cover most of the pavement types in College Station. Measurement spots were selected where the boundary of two or three materials could be clearly distinguished to accurately measure the GR. There was no shade with a full sun at all of the measuring points (Figure 3). A total of nine measurement spots were selected: Three spots for asphalt-concrete (A-C), two spots for asphalt-grass (A-G), two spots for concrete-grass (C-G), and two spots for asphalt-concrete-grass (A-C-G).

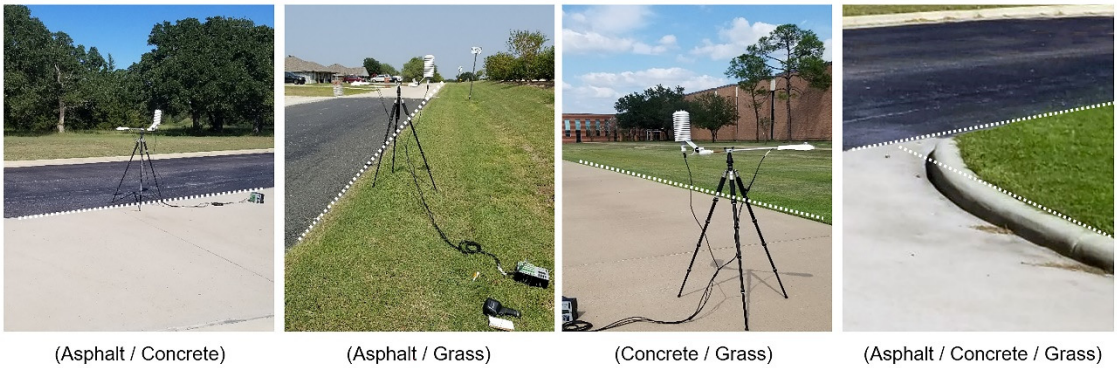

Figure 3. Various ground material conditions.

Field measurements were conducted for 16 days during the hot summer weather from 13 July to 19 September 2020. The measurement time was selected from 10 AM to 4 PM, a time of the day when people could easily be exposed to vulnerable thermal environments. To develop the model for various weather conditions, warm (29.4–31.6 °C), hot (31.7–35.0 °C), and very hot (over 35.0 °C), weather conditions were considered [26]. Measurements were conducted on sunny and mostly sunny days for accurate microclimatic data (Table 1).

Table 1. List of measurement days, time, max and min temperature, and sky conditions.

Date	Time	Ta (°C)		Sky Condition
		Max	Min	
13 July 2020	4–6 PM	38.33	37.79	Sunny
14 July 2020	4–6 PM	37.71	36.82	Sunny
3 August 2020	3–5 PM	36.86	36.37	Sunny
4 August 2020	3–5 PM	37.15	35.45	Sunny
13 August 2020	3–5 PM	38.92	38.58	Sunny
14 August 2020	12–2 PM	37.61	35.39	Sunny
15 August 2020	12–2 PM	37.68	35.37	Sunny
19 August 2020	11–1 PM	34.88	32.83	Sunny
20 August 2020	11–1 PM	34.57	33.73	Sunny
21 August 2020	12–2 PM	34.56	32.80	Sunny
23 August 2020	12–2 PM	35.94	33.12	Mostly Sunny
24 August 2020	11–1 PM	35.52	32.81	Mostly Sunny
25 August 2020	11–1 PM	31.90	29.32	Sunny
17 September 2020	4–6 PM	31.77	29.26	Mostly Sunny
18 September 2020	4–6 PM	31.75	30.24	Mostly Sunny
19 September 2020	4–6 PM	29.49	28.12	Sunny

2.2.1. Model Validation

To validate the model, this study compared the predicted terrestrial radiation (PTR) calculated by the model with the actual terrestrial radiation (ATR). In this case, ATR was measured simultaneously when measuring the microclimatic data for PTR for the nine measurement spots. For the A-C, A-G, and C-G, ATR was measured at a point where the GR value of the ground material was 0, 25, 50, 75, and 100% by moving the measuring point (Figure 4). For the A-C-G, ATR was measured at the midpoint, where the GR of asphalt, concrete, and grass are 25, 25, and 50%, respectively.

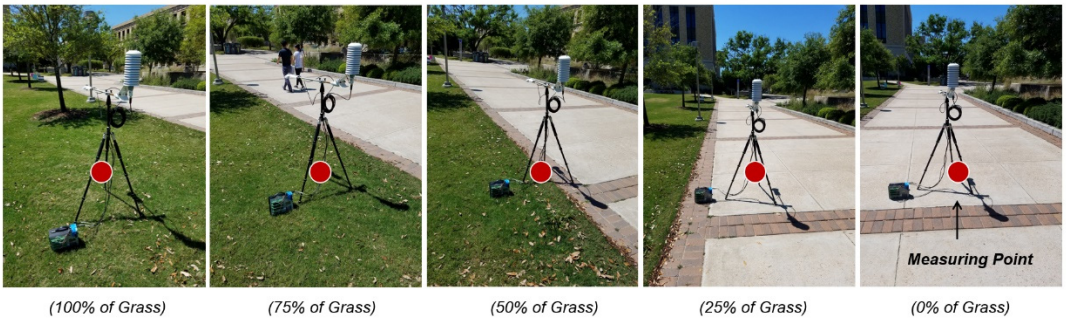

Figure 4. ATR measurement points.

2.2.2. Microclimatic Data

For the GRF-G model, this study measured the ground temperature to calculate the predicted terrestrial radiation by the GRF-G model (PTR-G). The ground temperature was measured vertically downward using the FLIR E6 thermal camera and Etekcity Infrared Thermometer 774. For the GRF-A model, this study measured the air temperature to calculate the predicted terrestrial radiation by the GRF-A model (PTR-A). The air temperature was measured by the HMP155A-L sensor at 5-s intervals. To validate the model, ATR was measured by the 4-component net radiometer (CNR4). The CNR4 radiometer measures the energy balance between the incoming short-wave and long-wave far infrared (FIR) radiation versus the surface-reflected short-wave and outgoing long-wave radiation. Finally, the CR3000 data logger was used to collect the data (Table 2). The HMP 155A-L sensor and CNR 4 radiometer were installed at 1.5 m above the ground.

Table 2. Microclimatic data measurement instruments.

Instruments	Microclimate Variables	Interval
HMP155A-L Sensor	Air Temperature	5 s
FLIR E6 Infrared Camera and Etekcity Infrared Thermometer 774	Ground (Surface) Temperature	1
CNR4 Net Radiometer	Terrestrial Radiation	5 s
CR3000	Data Logger	-

2.3. Data Analysis

To validate the model, this study compared the PTR with ATR. Pearson correlation analysis was used to analyze the relationship. The model can be validated when the relationship has a strong correlation with a statistically significant value at the 0.01 level. The analysis was conducted in two parts: (1) The PTR-G was compared with ATR to validate the GRF-G model and (2) the PTR-A was compared with ATR to validate the GRF-A model (Figure 5).

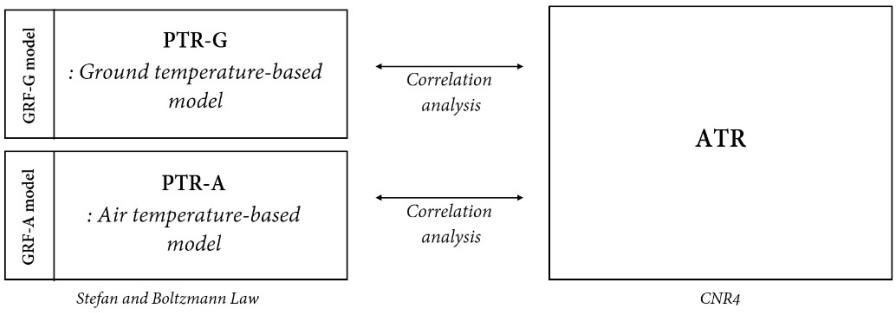

Figure 5. Concept of the analysis.

3. Results

3.1. Emissivity of the Ground Materials

Terrestrial radiation calculated by the Stefan-Boltzmann law should be multiplied by a correction factor called the emissivity. The emissivity of material indicates its effectiveness in emitting energy as thermal radiation. According to Brown and Gillespie [17], emissivity is always greater than 0.9 for items of interest in landscape design. Therefore, an uncorrected equation can usually be used when it is satisfied with the estimates within 10% of the reality. However, this study used the calculated emissivity values in the model for a more accurate PTR calculation. The emissivity of asphalt, concrete, and grass was calculated by comparing the PTR and ATR, and their results were 0.94, 0.96, and 0.98, respectively (Table 3).

Table 3. Emissivity and albedo of the ground materials.

	Asphalt (Avg)	Concrete (Avg)	Grass (Avg)
Emissivity	0.94	0.96	0.98
Albedo	0.06	0.28	0.19

3.2. GRF-G Model

Four models were developed to calculate PTRs for A-C, A-G, C-G, and A-C-G. The calculated PTRs were used in the model validation. Equation (5) is for A-C, Equation (6) is for A-G, Equation (7) is for C-G, and Equation (8) is for A-C-G. Emissivity of asphalt (0.94), concrete (0.96), and grass (0.98) was applied to the model.

$$R_T = Asphalt's\ GR \times 5.67 \times 10^{-8} \left(T_{Asphalt\_G} + 273\right)^4 \times 0.94 + Concrete's\ GR \times 5.67 \times 10^{-8} \left(T_{Concrete\_G} + 273\right)^4 \times 0.96 \quad (5)$$

$$R_T = Asphalt's\ GR \times 5.67 \times 10^{-8} \left(T_{Asphalt\_G} + 273\right)^4 \times 0.94 + Grass's\ GR \times 5.67 \times 10^{-8} \left(T_{Grass\_G} + 273\right)^4 \times 0.98 \quad (6)$$

$$R_T = Concrete's\ GR \times 5.67 \times 10^{-8} \left(T_{Concrete\_G} + 273\right)^4 \times 0.96 + Grass's\ GR \times 5.67 \times 10^{-8} \left(T_{Grass\_G} + 273\right)^4 \times 0.98 \quad (7)$$

$$R_T = Asphalt's\ GR \times 5.67 \times 10^{-8} \left(T_{Asphalt\_G} + 273\right)^4 \times 0.94 + Concrete's\ GR \times 5.67 \times 10^{-8} \left(T_{Concrete\_G} + 273\right)^4 \times 0.96 + Grass's\ GR \times 5.67 \times 10^{-8} \left(T_{Grass\_G} + 273\right)^4 \times 0.98 \quad (8)$$

where R_T is the predicted terrestrial radiation (W/m^2), GR is the ground ratio, $T_{Asphalt\_G}$ is the ground temperature of asphalt, $T_{Concrete\_G}$ is the ground temperature of concrete, and T_{grass_G} is the ground temperature of grass in Celsius degrees.

Table 4 shows the descriptive statistics of PTR-G and ATR. The samples for each measurement points were 51 for A-C, 46 for A-C, 44 for C-G, and 39 for A-C-G. For the A-C-G model, the mean of the PTR-G and ATR were 532.12 and 537.77 W/m^2, the SD of the PTR-G and ATR were 26.52 and 31.45 W/m^2, and the range of the PTR-G and ATR were from 507.66 to 609.70 W/m^2 and from 498.14 to 601.16 W/m^2, respectively. Other models for A-C, A-G, and C-G also showed a similar distribution. Overall, the results showed that the maximum, minimum, mean, and SD values of the PTR-G and ATR have very similar distributions.

Table 4. Descriptive statistics of the PTR-G and ATR.

Material		Max (W/m^2)	Mean (W/m^2)	Min (W/m^2)	SD (W/m^2)
A-C	PTR-G	659.69	574.80	521.00	37.21
	ATR	666.51	574.33	523.01	39.07
A-G	PTR-G	614.47	547.05	503.45	28.33
	ATR	628.66	550.34	506.91	32.80
C-G	PTR-G	560.77	518.49	491.47	17.74
	ATR	567.58	525.11	495.61	18.20
A-C-G	PTR-G	609.70	532.15	507.66	26.52
	ATR	601.16	537.77	498.14	29.45

3.3. GRF-A Model

To estimate the ground temperature using air temperature, regression analysis was used for each of the three ground materials [24,25]. Equations (9)–(11) showed the result of asphalt, concrete, and grass, respectively. R^2 values of asphalt, concrete, and grass were

0.762, 0.663, and 0.567, respectively. Moreover, three equations were statistically significant at the 0.01 level.

$$T_{asphalt} = -20 + 2 \times T_{air} \ (R^2 = 0.762, \ \ p < 0.01) \quad (9)$$

$$T_{concrete} = 8.5 + T_{air} \ (R^2 = 0.663, \ \ p < 0.01) \quad (10)$$

$$T_{grass} = 13 + 0.6 \times T_{air} \ (\mathrm{R}^2 = 0.567, \ \ p < 0.01) \quad (11)$$

where $T_{asphalt}$ is the predicted ground temperature of asphalt, $T_{concrete}$ is the predicted ground temperature of concrete, T_{grass} is the predicted ground temperature of grass, and T_{air} is the air temperature.

The ground temperature parts of the GRF-G model for each material were replaced by the equations created by the regression analysis, as follows:

$$\begin{gathered} R_T = Asphalt's\ GR \times 5.67 \times 10^{-8} \left((-20 + 2 \times T_{air}) + 273\right)^4 \times 0.94 + \\ Concrete's\ GR \times 5.67 \times 10^{-8} \left((8.5 + T_{air}) + 273\right)^4 \times 0.96 + Grass's\ GR \times \\ 5.67 \times 10^{-8} \left((13 + 0.6 \times T_{air}) + 273\right)^4 \times 0.98 \end{gathered} \quad (12)$$

where R_T is the terrestrial radiation ($\mathrm{W/m^2}$), GR is the ground ratio, and T_{air} is the air temperature in Celsius degrees.

Table 5 shows the descriptive statistics of PTR-A and ATR. The results of the ATR were the same as in the GRF-G section. For the A-C-G model, the mean of the PTR-A and ATR were 532.96 and 537.77 $\mathrm{W/m^2}$, the SD of the PTR-A and ATR were 20.39 and 29.45 $\mathrm{W/m^2}$, and the range of the PTR-A and ATR were from 488.90 to 563.10 $\mathrm{W/m^2}$ and from 498.14 to 601.16 $\mathrm{W/m^2}$, respectively. Other models for A-C, A-G, and C-G also showed a similar distribution. Overall, the value of the ATR is slightly higher than the PTR-A. According to the results, two values of the PTR-A and ATR showed similar distributions.

Table 5. Descriptive statistics of the PTR-A and ATR.

Material		Max ($\mathrm{W/m^2}$)	Mean ($\mathrm{W/m^2}$)	Min ($\mathrm{W/m^2}$)	SD ($\mathrm{W/m^2}$)
A-C	PTR-A	614.62	570.79	506.61	37.81
	ATR	666.51	574.33	523.01	39.07
A-G	PTR-A	582.65	545.19	491.42	32.51
	ATR	628.66	550.34	506.91	32.80
C-G	PTR-A	547.30	522.41	490.44	21.68
	ATR	567.58	525.11	495.61	18.20
A-C-G	PTR-A	563.10	532.96	488.90	20.39
	ATR	601.16	537.77	498.14	29.45

3.4. Model Validation

3.4.1. GRF-G Model

The results showed that the PTR-G and ATR were significantly positively correlated. The results of the correlation analysis are as follows: The correlation coefficients of the PTR-G and ATR for A-C, A-G, C-G, and A-C-G are 0.918, 0.924, 0.903, and 0.841, respectively (Figure 6, Table 6). Most of the researchers may agree that the correlation coefficients which are less than 0.1 are negligible and greater than 0.9, and represent a very strong correlation. However, the interpretation of various correlation coefficients between 0 and 1 is still controversial. Therefore, it is important that specific coefficients should be carefully interpreted as measuring the strength of the relationship in the context of the scientific questions presented [27].

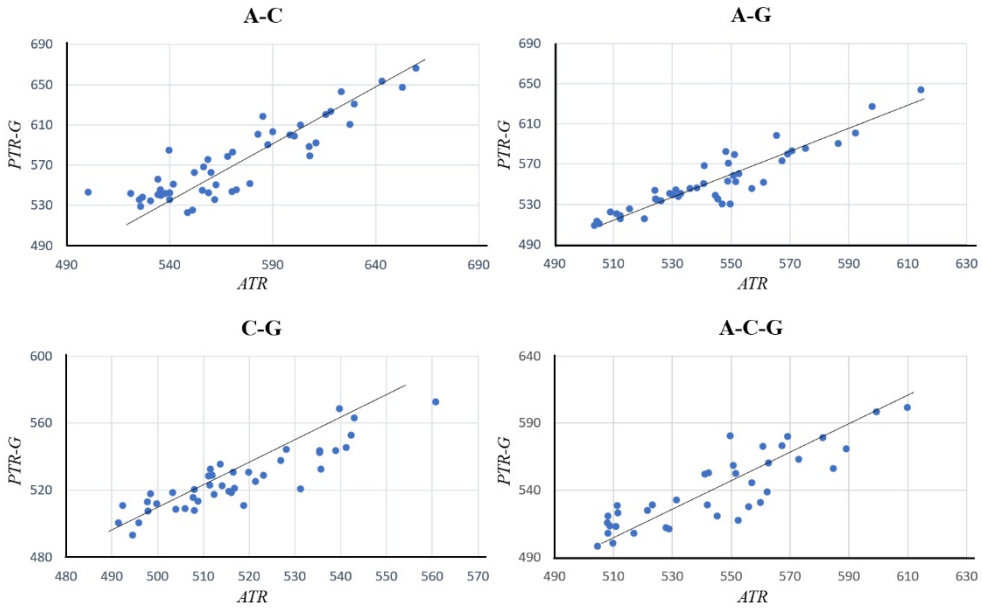

Figure 6. Correlation between the PTR-G and ATR.

Table 6. Correlation coefficient between the PTR-G and ATR.

	PTR-G (A-C)	PTR-G (A-G)	PTR-G (C-G)	PTR-G (A-C-G)
ATR	0.918 **	0.924 **	0.903 **	0.841 **

** Correlation is significant at the 0.01 level.

Schober et al. [27] attempted to interpret the correlation coefficients. They argued that if the absolute magnitude of the observed correlation coefficient is between 0.70 and 0.89, it shows that there is a strong correlation. Moreover, if the observed correlation coefficient is greater than 0.9, there is a very strong correlation. According to their definition, the results of this study showed that there is a strong or very strong correlation between the PTR-G and ATR (correlation coefficients = 0.841~0.924). All of the results were statistically significant at the 0.01 level. Therefore, the GRF-G model can be used for calculating the terrestrial radiation using the ground temperature for different ground conditions.

3.4.2. GRF-A Model

The results showed that there is a positive correlation between the PTR-A and ATR. The correlation coefficients of the PTR-A and ATR for A-C, A-G, C-G, and A-C-G are 0.781, 0.842, 0.821, and 0.779, respectively (Table 7). According to the definition of Schober et al. [27], there is a strong correlation between the PTR-A and ATR, which is statistically significant at the 0.01 level. Therefore, the GRF-A model can be used for calculating the terrestrial radiation of various ground conditions using the air temperature.

Table 7. Correlation coefficient between the PTR-A and ATR.

	PTR-A (A-C)	PTR-A (A-G)	PTR-A (C-G)	PTR-A (A-C-G)
ATR	0.781 **	0.842 **	0.821 **	0.779 **

** Correlation is significant at the 0.01 level.

4. Discussion

This study suggests the need to consider terrestrial radiation in thermal comfort measures to create MUD strategies. The findings indicate that terrestrial radiation is emitted differently depending on the proportion of different ground conditions. To recognize the need of terrestrial radiation, it is important to understand why terrestrial radiation is

important and how terrestrial radiation affects heat-related human health. Terrestrial radiation has a huge effect on human heat stress. As mentioned in the introduction, terrestrial radiation plays an important role in the outdoor human thermal comfort, which is defined as a state of mind that shows satisfaction with the thermal environment [28]. Previous studies have found that reducing the terrestrial radiation absorbed by a person improves the human thermal comfort [18,29,30].

High temperatures cause heat stress by making a person thermally uncomfortable. These thermal stresses cause heat-related health problems. Rohat et al. [31] showed that the heat stress risk, which is linked to the exposure to vulnerable people and extreme temperature events, such as heat hazard, resulted in heat-related health impacts. Moreover, Claudia et al. [32] assessed the heat stress effects on mortality. Their results showed that there is an increase in the number of outpatients and deaths on hot days by comparing days without thermal stress. Moreover, Kovats and Hajat [33] conducted a critical review on the relationship between heat stress and public health. Their results showed that heat stress causes heat-related illnesses (clinical signs), which eventually lead to heat death (Figure 7).

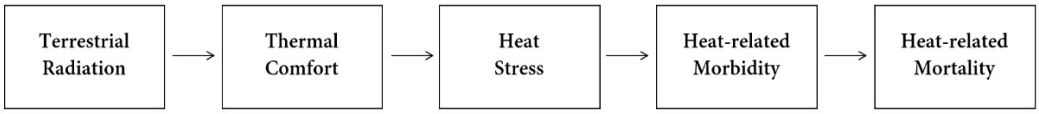

Figure 7. Causal chain from terrestrial radiation exposure to heat-related health.

This study simulated the energy budgets to demonstrate the effect of terrestrial radiation on human thermal comfort using the COMFA model proposed by Brown and Gillespie [17]. An example can be used to illustrate the importance of terrestrial radiation on a person's thermal comfort. Assume that the air temperature is 25 °C, the ground temperature is 35 °C, the human surface temperature is 25 °C, the ground material is grass, and a person is standing. The energy budget of terrestrial radiation emitted from the ground and absorbed by a person is 510 W/m^2. The energy budget refers to the degree of thermal comfort and the results showed that terrestrial radiation accounts for a significant portion of the total energy budget (Figure 8).

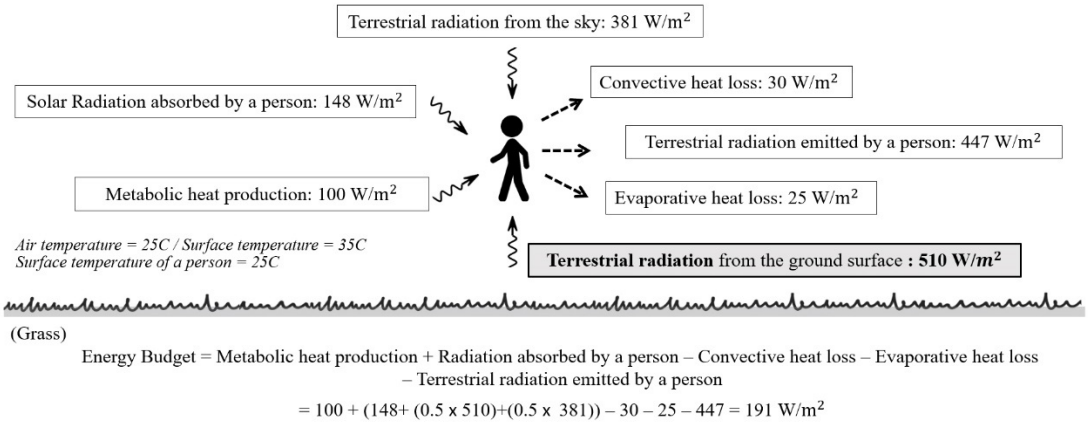

Figure 8. Energy budget calculation using the COMFA model.

There are no thermal comfort-related studies considering the different terrestrial radiation according to the different ground conditions. Therefore, this study is significant enough in conducting leading research on related issues through model development. This study developed two versions of the GRF model: The GRF-G model that can use ground temperature and the GRF-A model that can use air temperature. The models were developed with the theories and compared with actual measurements for validation. The result that both models have a statistically significant correlation between PTR and ATR

(correlation coefficients = about 0.8 ~ 0.9, $p < 0.01$) shows that it is theoretically possible to estimate terrestrial radiation through the models.

This study also found that when considering two different ground materials, the correlation between the PTR and ATR was higher than considering three ground materials. For the GRF-G model, the average coefficient of correlation analysis is 0.903 for two different materials and 0.810 for three different materials. For the GRF-A model, the average coefficient of correlation analysis is 0.814 for two different materials and 0.779 for three different materials at the 0.01 significant level. This indicates that the model is more accurate when considering fewer ground materials.

There are several limitations that need further research. When measuring the terrestrial radiation emitted from the ground using instruments, it is important to know how the instruments theoretically measure the terrestrial radiation and how terrestrial radiation is received by a real person. Ground temperature is usually measured vertically downward using a thermal camera (FLIR E6) or a pyrgeometer. Assuming that a person can be represented by a vertical cylinder, the terrestrial radiation from the ground (Figure 9A) should be translated into the amount of terrestrial radiation received by a vertical cylinder (Figure 9B).

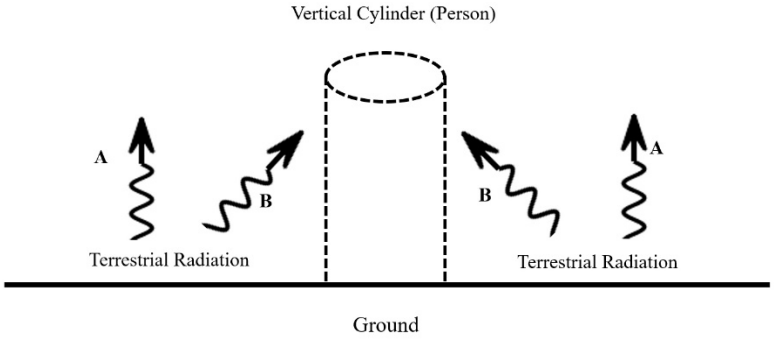

Figure 9. Concept of terrestrial radiation absorbed by a vertical cylinder.

The CNR4 upper longwave detector has a view of nearly 180° and the lower detector has a view of 150° (Figure 10). This indicates that it can measure all of the terrestrial radiation from the sky and ground hemisphere except for the space of 30°. It seems that the missing 30° might have only a minor effect on the amount of terrestrial radiation for a horizontal flat plate, but it might be quite important for a vertical cylinder. Therefore, further research needs to complement this limitation through theoretical and empirical grounds.

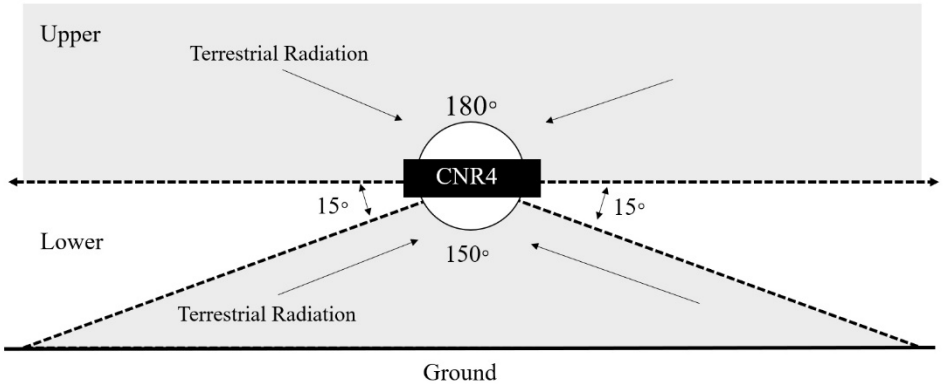

Figure 10. Concept of terrestrial radiation absorbed by CNR4.

Further research should also be conducted on a more accurate conversion using various methods and considering additional microclimate parameters. Ground temperature is

used to calculate the terrestrial radiation, which provides the most accurate value. However, ground temperature data have an issue in that data cannot be easily obtained relatively compared to the air temperature data. Therefore, previous studies attempted to estimate the ground temperature using the air temperature. This study used the regression analysis approach using only air temperature to estimate the ground temperature. In this study, the regression analysis was used. The results showed R^2 values of 0.762 for asphalt, 0.663 for concrete, and 0.573 for grass, respectively. This approach provides statistically significant results, but various methods for a more accurate conversion should be considered, which can include additional microclimate parameters. Many methods have been proposed to convert air temperature to ground temperature. Khan et al. [22] suggested the model for the asphalt ground temperature. In their model, various microclimate parameters, such as wind speed (m/s), air temperature (F), relative humidity, and solar radiation (W/m^2) were considered to estimate the ground temperature (F). According to their results, the model has an R^2 value of more than 0.9. Moreover, according to Diefenderfer et al. [34], their model included the daily maximum ambient temperature (°C), calculated daily solar radiation (W/m^2), and depth from the surface (m) to calculate the predicted daily maximum ground temperature (°C). Their adjusted R^2 value of the model was 0.771 for maximum temperature and 0.798 for minimum temperature. In addition, this study only considered air temperature and sky condition, while relative humidity and wind speed were not considered. Basically, relative humidity and wind speed can be theoretically similar when measuring terrestrial radiation for each measuring point. However, at the same time, they can affect the amount of terrestrial radiation delivered from the ground to the person. Therefore, to conduct a more accurate conversion, a further consideration of various methodologies is needed.

Additional models for various areas should be developed, since climate relationships and characteristics may vary depending on the location. According to the Köppen climate classification, climatic conditions vary depending on the region, continent, country, etc. As a pioneering research, this study was limited to the City of College Station, located in the Cfa climate zone (humid subtropical climate) for the increasing validity and reliability of the results, but additional research for different climatic zones is needed to use the GRF model in more diverse areas. The relationships between microclimate parameters vary depending on the climate zones. Mildrexler et al. [35] conducted a global analysis to compare air temperatures with land surface temperatures using satellite data of every World Meteorological Organization station on Earth. Their results showed that the relationship varied by latitude and longitude. Emissivity also varies across areas. Brown and Gillespie [17] found that most of the landscape design elements have a coefficient of 0.9 or more, thus when we are satisfied with the estimate of 10% of reality, we can use uncorrected equations. However, it is necessary to use more accurate emissivity values to measure the accurate terrestrial radiation. According to Wang et al. [36], even the same material may have different emissivity depending on changes in the temporal or spatial distribution. Therefore, further studies should consider various climates and seasonality considering the relationship between emissivity and terrestrial radiation.

Finally, for a better terrestrial radiation estimation, a wider range of ground materials, the consistent properties of each material, and securing more samples should be considered. This study considered only three materials: Asphalt, concrete, and grass. Soil was excluded due to the difficulty in securing a target site as it is a private issue. Therefore, additional ground materials need to be considered to apply the CRF model to various materials. Moreover, even if it is the same ground material, the characteristics of albedo and emissivity vary slightly depending on the different neighborhood environments. For example, according to the results of this study, grass has slightly different albedo and emissivity depending on the measurement spots since they have different grass conditions depending on their management status. These differences need to be considered for accurate research results. Furthermore, as a pioneering research, we tried to secure the sample number which can be statistically significant to present the need to consider different amounts of terrestrial

radiation. More than 30 samples were targeted and 51 for A-C, 46 for A-C, 44 for C-G, and 39 for A-C-G were used. However, further research will need to increase the samples and survey areas to achieve more accurate and statistically significant results.

5. Conclusions

Previous studies have not conducted sufficient research on the effect of terrestrial radiation on thermal comfort. This study conducted pioneering research on improving terrestrial radiation estimates for human energy budget models. The primary findings are as follows. First, this study presents the need to consider different terrestrial radiation estimates for human thermal comfort, since we found and validated that terrestrial radiation is emitted differently depending on the proportion of different ground conditions. Second, in order to improve terrestrial radiation estimates, this study argued that the ground ratio factor (GRF) concept should be considered. GRF represents the ratio of different ground materials, and GRF models were developed to estimate the different terrestrial radiation according to the different ground conditions. There are two models to use the ground and air temperature. The ground temperature-based GRF (GRF-G) model was developed using the Stefan-Boltzmann law for ground temperature usage and the air temperature-based GRF (GRF-A) model was developed using the regression analysis for air temperature usage. Third, the models were validated through a statistical analysis. Actual terrestrial radiation (ATR) was measured through a field measurement, which was used for the comparison with the predicted terrestrial radiation (PTR) from the models. The results showed that the PTR and ATR have a statistically significant strong correlation and this indicates that the model can be used to estimate terrestrial radiation.

In conclusion, these findings can be used to upgrade the existing human energy budget models by considering more diverse landscape design factors. This enables a more accurate measurement of human thermal comfort and development of microclimatic urban design (MUD) strategies to ameliorate thermal environments.

Author Contributions: Conceptualization, K.L. and R.D.B.; methodology, K.L. and R.D.B.; validation, K.L.; formal analysis, K.L.; investigation, K.L.; resources, K.L. and R.D.B.; data curation, K.L.; writing—original draft preparation, K.L. and R.D.B.; writing—review and editing, K.L. and R.D.B.; visualization, K.L.; supervision, R.D.B.; project administration, K.L. All authors have read and agreed to the published version of the manuscript.

Funding: This research received no external funding.

Institutional Review Board Statement: Not applicable.

Informed Consent Statement: Not applicable.

Conflicts of Interest: The authors declare no conflict of interest.

References

1. Memon, R.A.; Leung, D.Y.; Chunho, L. A review on the generation, determination and mitigation of urban heat island. *J. Environ. Sci.* **2008**, *20*, 120–128.
2. Zhao, X.; Liu, J.; Liu, L. Cool island effects of urban green open spaces in the process of urbanization: A multi-temporal study of Xiamen Island. In Proceedings of the 2016 4th International Workshop on Earth Observation and Remote Sensing Applications (EORSA), Guangzhou, China, 4–6 July 2016; pp. 363–367. [CrossRef]
3. Epstein, Y.; Moran, D.S. Thermal Comfort and the Heat Stress Indices. *Ind. Health* **2006**, *44*, 388–398. [CrossRef]
4. Abdel-Ghany, A.M.; Al-Helal, I.M.; Shady, M.R. Human Thermal Comfort and Heat Stress in an Outdoor Urban Arid Environment: A Case Study. *Adv. Meteorol.* **2013**, *2013*, 693541. [CrossRef]
5. Estoque, R.C.; Murayama, Y.; Myint, S.W. Effects of landscape composition and pattern on land surface temperature: An urban heat island study in the megacities of Southeast Asia. *Sci. Total Environ.* **2017**, *577*, 349–359. [CrossRef]
6. Mohammad, P.; Goswami, A.; Bonafoni, S. The Impact of the Land Cover Dynamics on Surface Urban Heat Island Variations in Semi-Arid Cities: A Case Study in Ahmedabad City, India, Using Multi-Sensor/Source Data. *Sensors* **2019**, *19*, 3701. [CrossRef] [PubMed]
7. Lenzholzer, S.; Brown, R.D. Post-positivist microclimatic urban design research: A review. *Landsc. Urban Plan.* **2016**, *153*, 111–121. [CrossRef]

8. Chen, D.; Wang, X.; Thatcher, M.; Barnett, G.; Kachenko, A.; Prince, R. Urban vegetation for reducing heat related mortality. *Environ. Pollut.* **2014**, *192*, 275–284. [CrossRef] [PubMed]
9. Gunawardena, K.R.; Wells, M.J.; Kershaw, T. Utilising green and bluespace to mitigate urban heat island intensity. *Sci. Total Environ.* **2017**, *584–585*, 1040–1055. [CrossRef]
10. Susca, T.; Gaffin, S.R.; Dell'Osso, G.R. Positive effects of vegetation: Urban heat island and green roofs. *Environ. Pollut.* **2011**, *159*, 2119–2126. [CrossRef] [PubMed]
11. Liu, Y.; Li, T.; Peng, H. A new structure of permeable pavement for mitigating urban heat island. *Sci. Total Environ.* **2018**, *634*, 1119–1125. [CrossRef] [PubMed]
12. Jenerette, G.D.; Harlan, S.L.; Stefanov, W.L.; Martin, C.A. Ecosystem services and urban heat riskscape moderation: Water, green spaces, and social inequality in Phoenix, USA. *Ecol. Appl.* **2011**, *21*, 2637–2651. [CrossRef] [PubMed]
13. Nakayama, T.; Hashimoto, S. Analysis of the ability of water resources to reduce the urban heat island in the Tokyo megalopolis. *Environ. Pollut.* **2011**, *159*, 2164–2173. [CrossRef] [PubMed]
14. Vahmani, P.; Jones, A. Water conservation benefits of urban heat mitigation. *Nat. Commun.* **2017**, *8*, 1072. [CrossRef] [PubMed]
15. Johansson, E.; Emmanuel, R. The influence of urban design on outdoor thermal comfort in the hot, humid city of Colombo, Sri Lanka. *Int. J. Biometeorol.* **2006**, *51*, 119–133. [CrossRef] [PubMed]
16. Yang, W.; Wong, N.H.; Li, C.-Q. Effect of Street Design on Outdoor Thermal Comfort in an Urban Street in Singapore. *J. Urban Plan. Dev.* **2016**, *142*, 05015003. [CrossRef]
17. Brown, R.D.; Gillespie, T.J. *Microclimatic Landscape Design: Creating Thermal Comfort and Energy Efficiency*; John Wiley & Sons: New York, NY, USA, 1995; Volume 1.
18. Shahidan, M.F.; Shariff, M.K.; Jones, P.; Salleh, E.; Abdullah, A.M. A comparison of *Mesua ferrea* L. and *Hura crepitans* L. for shade creation and radiation modification in improving thermal comfort. *Landsc. Urban Plan.* **2010**, *97*, 168–181. [CrossRef]
19. Nouri, A.S.; Costa, J.P.; Santamouris, M.; Matzarakis, A. Approaches to Outdoor Thermal Comfort Thresholds through Public Space Design: A Review. *Atmosphere* **2018**, *9*, 108. [CrossRef]
20. Staiger, H.; Laschewski, G.; Matzarakis, A. Selection of Appropriate Thermal Indices for Applications in Human Biometeorological Studies. *Atmosphere* **2019**, *10*, 18. [CrossRef]
21. Coccolo, S.; Kämpf, J.; Scartezzini, J.-L.; Pearlmutter, D. Outdoor human comfort and thermal stress: A comprehensive review on models and standards. *Urban Clim.* **2016**, *18*, 33–57. [CrossRef]
22. Khan, Z.H.; Islam, R.; Tarefder, R.A. Determining asphalt surface temperature using weather parameters. *J. Traffic Transp. Eng.* **2019**, *6*, 577–588. [CrossRef]
23. Shamsipour, A.A.; Azizi, G.; Ahmadabad, M.K.; Moghbel, M. Surface temperature pattern of asphalt, soil, and grass in different weather condition. *J. Biodivers. Environ. Sci* **2013**, *3*, 80–89.
24. Ariawan, I.M.A.; Subagio, B.S.; Setiadji, B.H. Development of Asphalt Pavement Temperature Model for Tropical Climate Conditions in West Bali Region. *Procedia Eng.* **2015**, *125*, 474–480. [CrossRef]
25. Barman, D.; Kundu, D.; Pal, S.; Pal, S.; Chakraborty, A.; Jha, A.; Mazumdar, S.; Saha, R.; Bhattacharyya, P. Soil temperature prediction from air temperature for alluvial soils in lower Indo-Gangetic plain. *Int. Agrophysics* **2017**, *31*, 9–22. [CrossRef]
26. Shak, G.L.; Scarpa, M.; Knudsen, C.G. Temperature Terminology for Public Forecasts. *Weatherwise* **1966**, *19*, 161–163. [CrossRef]
27. Schober, P.; Boer, C.; Schwarte, L.A. Correlation coefficients: Appropriate use and interpretation. *Anesth. Analg.* **2018**, *126*, 1763–1768. [CrossRef]
28. Xu, M.; Hong, B.; Mi, J.; Yan, S. Outdoor thermal comfort in an urban park during winter in cold regions of China. *Sustain. Cities Soc.* **2018**, *43*, 208–220. [CrossRef]
29. Brown, R.D. Ameliorating the effects of climate change: Modifying microclimates through design. *Landsc. Urban Plan.* **2011**, *100*, 372–374. [CrossRef]
30. Picot, X. Thermal comfort in urban spaces: Impact of vegetation growth: Case study: Piazza della Scienza, Milan, Italy. *Energy Build.* **2004**, *36*, 329–334. [CrossRef]
31. Rohat, G.; Flacke, J.; Dosio, A.; Pedde, S.; Dao, H.; van Maarseveen, M. Influence of changes in socioeconomic and climatic conditions on future heat-related health challenges in Europe. *Glob. Planet. Chang.* **2018**, *172*, 45–59. [CrossRef]
32. Di Napoli, C.; Pappenberger, F.; Cloke, H.L. Assessing heat-related health risk in Europe via the Universal Thermal Climate Index (UTCI). *Int. J. Biometeorol.* **2018**, *62*, 1155–1165. [CrossRef]
33. Kovats, R.S.; Hajat, S. Heat stress and public health: A critical review. *Annu. Rev. Public Health* **2008**, *29*, 41–55. [CrossRef] [PubMed]
34. Diefenderfer, B.K.; Al-Qadi, I.L.; Diefenderfer, S.D. Model to predict pavement temperature profile: Development and validation. *J. Transp. Eng.* **2006**, *132*, 162–167. [CrossRef]
35. Mildrexler, D.J.; Zhao, M.; Running, S.W. A global comparison between station air temperatures and MODIS land surface temperatures reveals the cooling role of forests. *J. Geophys. Res. Space Phys.* **2011**, *116 (G3)*, 1–15. [CrossRef]
36. Wang, K.; Wan, Z.; Wang, P.; Sparrow, M.; Liu, J.; Zhou, X.; Haginoya, S. Estimation of surface long wave radiation and broadband emissivity using Moderate Resolution Imaging Spectroradiometer (MODIS) land surface temperature/emissivity products. *J. Geophys. Res. Space Phys.* **2005**, *110 (D11)*, 1–12. [CrossRef]